

Mildly boosted dark matter annihilation and reconciling indirect galactic signals

Steven J. Clark*

Hood College, Frederick, MD 21701, USA

The galactic center excess is a possible non-gravitational observation of dark matter; however, the canonical dark matter model (thermal freeze-out) is in conflict with other gamma-ray observations, in particular those made of the Milky Way’s satellite dwarf galaxies. Here we consider the effects of a two-component dark matter model which results in minimally boosted particles that must remain bound to their host galaxy in order to produce an observational signal. This leads to a signal that is heavily dependent on galactic scale and can help reconcile the differences in the galactic center and dwarf galaxy measurements under the dark matter paradigm.

INTRODUCTION

The galactic center excess (GCE) [1–3] is a flux of gamma rays originating from the center of the Milky Way galaxy that is higher than predictions from astrophysical processes. One possible interpretation is that it is due to dark matter (DM) interactions with Standard Model particles (SM); if correct, this interpretation would be the first non-gravitational detection of DM [4–6]. However, the DM parameter space that best correlates with the DM interpretation is also in conflict with other measurements; in particular, it is in conflict with similar gamma-ray measurements of the Milky Way’s satellite spherical dwarf galaxies (dSph) [7–12].

If the GCE does originate from DM interactions, then reconciling these two observations can shed light on DM properties. Multiple models have attempted to address this difference in light of the DM proposal. Approaches frequently revolve around modifying the SM spectra through different particle productions [13, 14] and adjusting the astrophysical interaction rates (commonly termed the J-factor). Some approaches for altering the J-factor include interactions with various velocity dependencies [15–20] or signals originating from secondary highly boosted DM [21–24]. For approaches that modify the J-factor, the central concept is that there is an inherent difference in the two environments (small and large galaxies) which leads to galactic dependencies not captured in the canonical value [24]. In order to reconcile the GCE and dSph signals, this would require either an enhancement in larger galaxies or a suppression in smaller ones.

Expanded dark sectors offer a possible approach at addressing these signals by introducing dynamics that play a crucial role in DM distributions. Note that galactic DM is non-relativistic; this implies that processes that impart small increases to a particle’s kinetic energy, compared with its rest mass, can lead to the particle achieving escape velocity, v_{esc} , from the host galaxy. Because v_{esc} is dependent on galactic size, the requisite energy is lower in smaller galaxies and thus easier to escape. If this “boosted” DM particle is SM active, larger fractions of escaping boosted DM correspond with lower observa-

tional galactic signals. This leads to an overall suppression in the observed rates that is more pronounced in smaller galaxies, thus providing a mechanism to reconcile the GCE and dSph results.

In this work, we investigate galactic signal rates from multi-component DM models where the SM active components are created with a mild boost from a dominant SM inert portion. These types of models lead to a strong galactic dependence in observational rates with a rapid transition where galaxies above a critical scale experience minimal alterations to canonical rates while those below can experience strong to total suppression.

MODEL AND BOUNDED FRACTION

For illustrative purposes, we consider a basic two component dark matter toy model similar to [24] consisting of χ_1 and χ_2 with mass relationships $m_1 > m_2$ and $m_1/m_2 \approx 1$. χ_1 annihilates to χ_2 while χ_2 annihilates to standard model particles.

$$\chi_1\chi_1 \rightarrow \chi_2^b\chi_2^b \quad (1)$$

$$\chi_2\chi_2 \rightarrow \text{SM} \quad (2)$$

where the “b” superscript indicates that the χ_2 s are produced with extra kinetic energy. We assume χ_1 annihilation is weak allowing for χ_1 to serve as the dark matter candidate while the χ_2 annihilation rate is comparatively much stronger. From the perspective of a galaxy, χ_1 s comprise the majority of the dark matter, and χ_2 s are produced through χ_1 annihilation. These χ_2 will either be produced with sufficient velocity to overcome the gravitational potential and escape the galaxy, or they will remain bound. We will assume that if they achieve escape velocity, the χ_2 annihilation coupling is small enough that they escape without further interaction (for annihilation occurring while escaping the galaxy, see Ref. [24]). If χ_2 s do not achieve escape velocity, they persist in the host galaxy until they annihilate with another χ_2 . In this setup, the galactic χ_2 population fluctuates until it reaches a steady state solution, balancing between χ_2 injections from the first interaction (Eq. (1) adjusted by the fraction that escape the galaxy) and depletion from

the second annihilation (Eq. (2)) producing a SM signal similar to canonical DM annihilation.¹ For this work, we assume that cross-sections are sufficient for all galaxies to reach this equilibrium state. The observable signal is directly proportional to the rate of χ_2 annihilation, and when at equilibrium, it is also proportional to the χ_2 injection rate.

Two quantities are required to determine the rate of χ_2 injection into the host galaxy: the base rate of χ_1 annihilation producing χ_2 s and the χ_2^b fraction from any particular χ_1 annihilation that does not achieve escape velocity. We first discuss the fraction that does not reach v_{esc} . Fig. (1) shows χ_1 annihilation in the center of mass frame (COM). $v_{1,2}$ corresponds to the velocity of $\chi_{1,2}$ in the frame while v_c is the velocity of the center of mass with respect to the galactic frame. θ is the angle between v_c and v_2 .

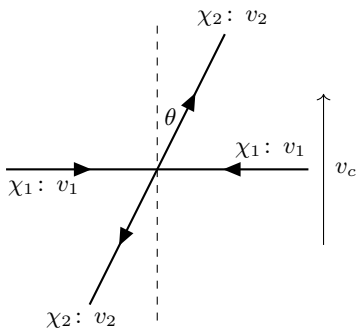


Figure 1. χ_1 annihilation in the center of mass (COM) frame. Annihilation products that move in the same direction as the COM receive an increase to their velocity when converting to the galactic reference frame while those moving in the opposite direction are decreased. Depending on v_2 , v_c , and the gravitational potential Φ , a minimum θ is required to remain bound to the galaxy. If the boosting velocity is too large, all χ_2 particles achieve v_{esc} .

Using conservation of energy, it is easy to show that

$$\begin{aligned} v_2^2 &= v_1^2 + \left(1 - \frac{v_1^2}{c^2}\right) \left(1 - \frac{m_2^2}{m_1^2}\right) c^2 \\ &= v_1^2 + \Delta v^2 \end{aligned} \quad (3)$$

where $\Delta v^2 \approx (1 - m_2^2/m_1^2) c^2$ in the non-relativistic limit. In the COM frame, both χ_2 s have the same velocity; however, in the galactic reference frame, a difference develops depending on their orientation with v_c . In the galactic frame, denoted by subscript “g”, the daughter particle velocity is

$$v_{2,g}^2 = v_2^2 + v_c^2 + 2v_2v_c \cos \theta \quad (4)$$

where we have assumed that all velocities are non-relativistic. It should also be noted that in the non-relativistic limit $v_1 = v_r/2$ where v_r is the relative velocity between the two parent χ_1 particles. This is true for both the COM and galactic reference frames.

For χ_2 to remain bound to the galaxy, the total energy must be negative; this leads to the relationship $\Phi + v_{2,g}^2/2 < 0$ where Φ is the gravitational potential of the host galaxy. Combining this relationship with Eqs. (3) and (4) as well as $v_1 = v_r/2$, we arrive at the condition

$$\cos \theta < \cos \theta_{\text{min}} = -\frac{2\Phi + v_c^2 + v_r^2/4 + \Delta v^2}{2v_c \sqrt{v_r^2/4 + \Delta v^2}} \quad (5)$$

where θ_{min} is the minimum angle that v_2 must make with v_c in order for the χ_2 to remain bound to the galaxy. If the right hand side of Eq. (5) is greater than 1, then the condition is always satisfied, all products are bound, and $\cos \theta_{\text{min}} = 1$; if it is less than -1 , $\cos \theta_{\text{min}} = -1$ and all products escape. Note that Eq. (5) is valid only for $v_c > 0$. For $v_c = 0$, the binding condition is $-2\Phi > v_r^2/4 + \Delta v^2$; otherwise, all products escape.

For simplicity, we assume that χ_1 annihilation is isotropic in the COM frame. In this isotropic example, the bound on $\cos \theta$ translates to the fraction of bounded annihilation products (f_{bound}) through the fractional area of a 2-sphere between $\theta_{\text{min}} \leq \theta \leq \pi$.

$$f_{\text{bound}} = \frac{1}{2} \int_{\theta_{\text{min}}}^{\pi} \sin \theta \, d\theta = \frac{1 + \cos \theta_{\text{min}}}{2} \quad (6)$$

INITIAL ANNIHILATION RATE

To determine the initial annihilation rate from χ_1 , we follow the approach from Ref. [18] with the addition of f_{bound} as discussed above to restrict the effective rate to include just the fraction of daughter particles which remain bound to the galaxy. For this work, the relevant quantity is $P_n^2(\hat{r})$. In canonical velocity independent annihilation rates, $P_n^2(\hat{r})$ is analogous to the square of the DM density (ρ^2) and evaluated from the DM velocity distribution, capturing the relative rate of annihilation occurring at a particular position in the galaxy.

$$\begin{aligned} P_n^2(\hat{r}) &\equiv \int d^3\hat{v}_1 d^3\hat{v}_2 |\hat{v}_1 - \hat{v}_2|^n \\ &\quad \times \hat{f}(\hat{r}, \hat{v}_1) \hat{f}(\hat{r}, \hat{v}_2) f_{\text{bound}}(\hat{v}_1, \hat{v}_2, \Delta\hat{v}) \\ &= 8\pi^2 \int_0^\infty d\hat{v}_1 \int_0^\infty d\hat{v}_2 \int_{|\hat{v}_1 - \hat{v}_2|}^{\hat{v}_1 + \hat{v}_2} d\hat{v}_r \hat{v}_1 \hat{v}_2 \hat{v}_r^{n+1} \\ &\quad \times \hat{f}(\hat{r}, \hat{v}_1) \hat{f}(\hat{r}, \hat{v}_2) f_{\text{bound}}(\hat{v}_1, \hat{v}_2, \hat{v}_r, \Delta\hat{v}) \end{aligned} \quad (7)$$

Subscripts correspond to the two individual parent χ_1 particles involved in the annihilation. (Note that this

¹ Because χ_2 will only experience a mild boost, their annihilation spectra will be identical to similar final products as canonical DM annihilation.

differs from the preceding section where subscripts indicated different particle species.) $\hat{f}(\hat{r}, \hat{v})$ is the phase-space distribution for χ_1 in the galaxy assumed here to be isotropic. $\hat{v}_r = |\hat{\mathbf{v}}_1 - \hat{\mathbf{v}}_2|$ is the relative velocity between the two parent particles with n being a model parameter. $f_{\text{bound}}(\hat{v}_1, \hat{v}_2, \hat{v}_r, \Delta\hat{v}) = f_{\text{bound}}(\hat{\mathbf{v}}_1, \hat{\mathbf{v}}_2, \Delta\hat{v})$ is the fraction of χ_2 daughters bound to the host galaxy in an annihilation. Also note the relationship $4\hat{v}_c + \hat{v}_r = 2(\hat{v}_1 + \hat{v}_2)$.

For convenience in analyzing multiple galaxies later in this work, we have introduced the scaled distances, densities, and velocities in Eq. (7)

$$\hat{r} \equiv \frac{r}{r_s}, \quad \hat{\rho} \equiv \frac{\rho}{\rho_s}, \quad \text{and} \quad \hat{v} \equiv \frac{v}{\sqrt{4\pi G \rho_s r_s^2}} \quad (8)$$

where r_s and ρ_s are the galactic scale and density parameters, and G is the gravitational constant. Furthermore, the scaled phase-space distribution and gravitational potential are

$$\hat{f}(\hat{r}, \hat{v}) = (4\pi G)^{3/2} \rho^{1/2} r_s^3 f(r, v) \quad (9)$$

$$\hat{\Phi} = \frac{\Phi}{4\pi G \rho_s r_s^2} \quad (10)$$

where $\hat{\rho}(\hat{r}) = \int d^3v \hat{f}(\hat{r}, \hat{v})$.

As stated before, Eq. (7) encapsulates the relative rate of DM annihilation, and n captures the velocity dependence. For this work, we consider only the velocity independent interaction $n = 0$ and leave $n \neq 0$ for future studies. For $n = 0$ and $f_{\text{bound}} = 1$, Eq. (7) reduces to $\hat{\rho}^2$ as expected.

J-factors (a measure of the expected flux) adjust the annihilation rate by accounting for the distance to the object and the observation window through a line of sight (l.o.s.) and region of interest (ROI) integration over P_n^2 .

$$\text{J-factor} = \rho_s^2 \int_{\text{l.o.s.}} dl \int_{\text{ROI}} d\Omega P_n^2(r/r_s) \quad (11)$$

Potentials and Phase-Space Distributions

From a known DM distribution, the potential can be calculated using Newtonian gravity. If the distribution is spherically symmetric, then the scaled potential is [18, 25, 26]

$$\hat{\Phi}(\hat{r}) = - \int_{\hat{r}}^{\infty} \frac{dx}{x^2} \int_0^x dy y^2 \hat{\rho}(y) \quad (12)$$

In addition, if the DM velocity distribution is assumed to be isotropic and the halo is in equilibrium, the velocity distribution can also be determined from the density and the potential in terms of E , the energy per unit mass through [18]

$$\hat{f}(\hat{E}) = \frac{1}{\sqrt{8\pi^2}} \int_{\hat{E}}^0 \frac{d^2\hat{\rho}}{d\hat{\Phi}^2} \frac{d\hat{\Phi}}{\hat{\Phi} - \hat{E}} \quad (13)$$

$$\hat{E}(\hat{r}, \hat{v}) = \frac{E}{4\pi G \rho_s r_s^2} = \frac{\hat{v}^2}{2} + \hat{\Phi}(\hat{r}) \quad (14)$$

where we assume v and E go to zero at $r = \infty$. In this manner, we are able to define a fully self-consistent velocity distribution for the DM halo. The density can be found from the velocity distribution through

$$\hat{\rho}(\hat{r}) = 4\pi \int_0^{\sqrt{-2\hat{\Phi}(\hat{r})}} d\hat{v} \hat{v}^2 \hat{f}(\hat{r}, \hat{v}) \quad (15)$$

$$= 4\sqrt{2}\pi \int_{\hat{\Phi}(\hat{r})}^0 d\hat{E} \hat{f}(\hat{E}) \sqrt{\hat{E} - \hat{\Phi}(\hat{r})} \quad (16)$$

where $\hat{f}(\hat{E}) = \hat{f}(\hat{r}, \hat{v})$. For this work, we assume the NFW profile $\hat{\rho}(\hat{r}) = \{\hat{r}(1 + \hat{r}^2)\}^{-1}$ [27] for all galaxies. This leads to the gravitation potential $\hat{\Phi}(\hat{r}) = -\ln(1 + \hat{r})/\hat{r}$ where $\ln(x)$ is the natural logarithm. From $\hat{\rho}(\hat{r})$ and $\hat{\Phi}(\hat{r})$, we solve for $\hat{f}(\hat{r}, \hat{v})$ numerically.

ADJUSTED ANNIHILATION RATES

Due to the boost received during the first annihilation, only a fraction of χ_2 remains bound to the galaxy. Fig. (2) shows $P_n^2/\hat{\rho}^2$ for various kick velocities. The ratio between $P_n(\hat{r})^2$ and $\rho(\hat{r})^2$ is effectively the number of χ_2 daughters that remain bound to the galaxy and the number that are produced. This ratio captures the fraction of the first annihilation products that are bound to the galaxy and which can participate in future interactions.

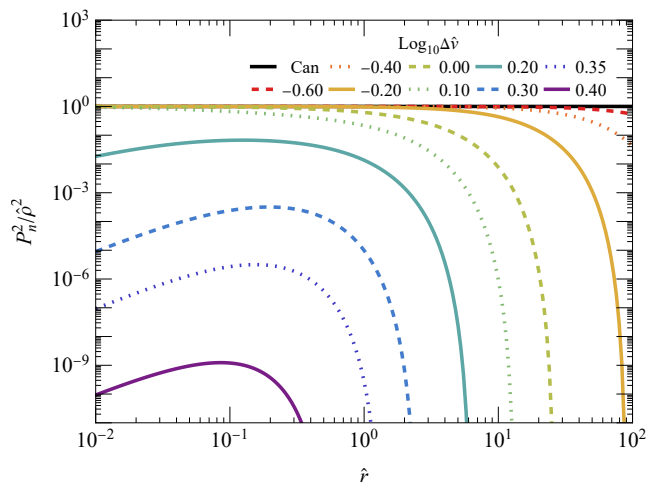


Figure 2. Fraction of χ_2 products from a χ_1 annihilation that remain gravitationally bound to the host galaxy ($P_n^2/\hat{\rho}^2$) for various kick velocities, $\Delta\hat{v}$. “Can” refers to the canonical dark matter model with $P_n^2 = \hat{\rho}^2$ and is also equal to the total number of χ_1 annihilation events in all models. As $\Delta\hat{v}$ increases, the level of suppression increases at all scales with larger radial distances more strongly affected. For $\Delta\hat{v} \gtrsim 1$, shorter distances also become heavily suppressed due to a lack of v_c to allow adequate back-scattering. At $\Delta\hat{v} = \sqrt{8}$, all annihilation products escape the galaxy.

As would be expected from Eqs. (3 - 5), for $\Delta\hat{v} \ll 1$, all products remain in the host galaxy. This is due to the

minimal changes to the energy distribution in the system. As $\Delta\hat{v}$ increases, escape occurs at large galactic radii due to the lower gravitational potential where even a small velocity change can provide the required energy. With increasing $\Delta\hat{v}$, the outer edges continue to become suppressed with the development of a critical radius above which there is total suppression.

This total suppression is due to the kick velocity providing the required energy for all valid velocity combinations to escape at the particular radius. From Eq. (4), $v_{c,\max}(r) = \Phi(r)$, and $\cos\theta = -1$, it is easy to find this maximum kick velocity where all annihilation products are unbound from the galaxy,

$$\Delta\hat{v}_{\max}^2 < -8\hat{\Phi}. \quad (17)$$

For each curve shown in Fig. (2), this value is observed by the location of the sharp right cutoff.

This pattern continues until $\Delta\hat{v} \approx 1$ where increased suppression begins at small radii. This suppression is due to a lack of v_c to allow for back-scattering events ($\cos\theta < 0$) that sufficiently reduce their energy. At $\Delta\hat{v} = \sqrt{2}$, the increase in kinetic energy is equal to the deepest portion of the NFW potential. This requires all bound products to be back-scattered with respect to v_c in order to reduce their speed. The amount of energy reduction in back-scattering is more pronounced for larger v_c . At small galactic radii in the NFW distribution, a large proportion of the velocity distribution has low velocities compared with distributions at larger radii. This results in parent particles having lower average v_c at small radii, leading to an incapability to sufficiently back-scatter to keep products bound to the galaxy even with the larger gravitational potential. Instead, these back-scattering events still have sufficient energy to escape. Rates at small radii thus experience a more dramatic suppression when compared to larger distances, and a peak in the rates is introduced for large $\Delta\hat{v}$ as observed in Fig. (2).

For $\Delta\hat{v}^2 > -8\hat{\Phi}_{\max}$, all products escape and the galaxy is completely suppressed to 0. For the NFW profile, this kick velocity corresponds to $\Delta\hat{v}_{\max, \text{NFW}}^2 = 8$ ($\log_{10} \Delta\hat{v}_{\max, \text{NFW}} \approx 0.45$).

Total Rates

The total scaled annihilation rate for a galaxy can be found through $\int d^3\hat{r} P_n^2(\hat{r}) = P_{n, \text{tot}}^2$. In Fig. (3), we show the ratio between the galactic rate and the canonical result for the NFW distribution. Due to the assumption that χ_1 and χ_2 are in equilibrium, this ratio is equal to the change in expected signal from the second annihilation and the canonical result. For $\Delta\hat{v} \ll 1$, there is minimal variation from the canonical result as expected. At $\Delta\hat{v} \approx 0.5$, the rate begins to dramatically decrease such that it is negligible by $\Delta\hat{v} \approx 2$. At $\Delta\hat{v} = \sqrt{-8\hat{\Phi}_{\max}}$, the

rate reaches zero as no annihilation products are bound to the galaxy. As discussed earlier, for the NFW distribution, this occurs at $\Delta\hat{v} = \sqrt{8} \approx 2.83$.

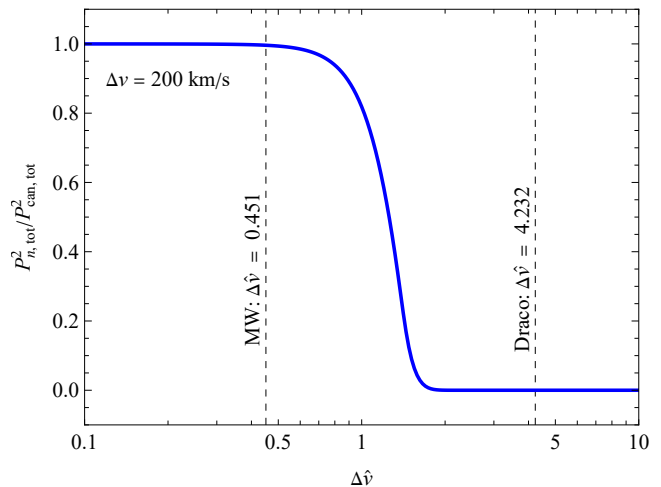


Figure 3. Ratio between the total injection rate of bound χ_2 daughter particles from χ_1 annihilation ($P_{n, \text{tot}}^2$) and the canonical annihilation rate. For $\Delta\hat{v} \ll 1$, the two are identical; however, there is a sharp drop at $\Delta\hat{v} \approx 1$ and the ratio reaches zero (no bound χ_2 are injected) at $\Delta\hat{v} = \sqrt{8}$ for the NFW distribution. Also shown are $\Delta\hat{v}$ for the Milky Way (MW) and Draco galaxies for $\Delta v = 200$ km/s. For this value of Δv , MW is close to the canonical result while Draco is deep in the totally suppressed regime. Other commonly studied dSph have $\Delta\hat{v}$ similar to Draco and would also be totally suppressed.

For a single model, the kick velocity (Δv) will be constant for all galaxies; however, scaled velocities ($\Delta\hat{v}$) are galaxy dependent. Due to the sharp transition from full canonical expectations and a complete reduction to zero, some galaxies may experience almost no variation while others could experience dramatic departures from the canonical value. The main contributor to how different galaxies behave is their physical dimensions. In Fig. (3), we have included $\Delta\hat{v}$ for the Milky Way (0.451) and the dwarf galaxy Draco (4.232) assuming $\Delta v = 200$ km/s.² For this choice of Δv , we would expect minimal alterations from the canonical signal for the Milky Way while expecting a complete suppression from Draco. Similar results will occur for other dSph galaxies. This suppression could account for the discrepancy between GC and Fermi dSph measurements.

Observing a signal from the Milky Way while experiencing a departure from the canonical result for dSph necessitates $\Delta v \sim 10 - 500$ km/s, which corresponds to a

² For the Milky Way (Draco), we used $\rho_s = 0.345$ (2.96) GeV/cm³ and $r_s = 20$ (0.728) kpc. [28] Other dSph galaxies commonly used in dark matter searches have similar values to Draco ($4 < \Delta\hat{v} < 6$).

mass splitting $\Delta m/m_1 \sim 10^{-9} - 10^{-6}$. This range is at the extreme of expected differences; a more conservative range would be $\Delta m/m_1 \sim 10^{-8} - 10^{-7}$ to allow for a sizable Milky Way signal while experiencing large variations from the canonical result for dSphs. Interestingly, this is the same mass splitting range as the 2cDM model needed to explain the missing galaxy, core-cusp, and too-big-to-fail problems of N -body simulations [29–31]; this is not completely unexpected due to the similarity in the models.

Care should be taken when interpreting these results, however, as they are a measure of the total annihilation rate of the galaxy. When converting to J -factors, they will be most accurate for distant galaxies, which the Milky Way is not. Further work is needed to understand how the secondary annihilation distribution in the galaxy will differ from canonical annihilation to identify if there are additional features when considering the angular J -factor along with the effect of galactic DM overdensities. In addition, more work is needed to better understand the equilibrium requirements necessary to reach the steady state situation assumed here and how it can differ in galactic environments.

Overall, this model introduces a mechanism that can explain the GCE as well as the lack of an observation in dSph under the DM interpretation. A characteristic feature to distinguish it from other models is a dramatic drop in excess SM products at a critical galactic scale. If measured, this scale can be used to measure the mass splitting between the two DM species.

ACKNOWLEDGEMENTS

We thank Bhaskar Dutta and Savvas Koushiappas for helpful discussion and suggestions in the preparation of this work.

* sclark@hood.edu

- [1] L. Goodenough and D. Hooper, “Possible Evidence For Dark Matter Annihilation In The Inner Milky Way From The Fermi Gamma Ray Space Telescope,” [arXiv:0910.2998](https://arxiv.org/abs/0910.2998) [hep-ph].
- [2] D. Hooper and L. Goodenough, “Dark Matter Annihilation In The Galactic Center As Seen by the Fermi Gamma Ray Space Telescope,” *Phys. Lett. B* **697** (2011) 412–428, [arXiv:1010.2752](https://arxiv.org/abs/1010.2752) [hep-ph].
- [3] **Fermi-LAT** Collaboration, M. Ackermann *et al.*, “The Fermi Galactic Center GeV Excess and Implications for Dark Matter,” *Astrophys. J.* **840** no. 1, (2017) 43, [arXiv:1704.03910](https://arxiv.org/abs/1704.03910) [astro-ph.HE].
- [4] F. Calore, I. Cholis, and C. Weniger, “Background Model Systematics for the Fermi GeV Excess,” *JCAP* **03** (2015) 038, [arXiv:1409.0042](https://arxiv.org/abs/1409.0042) [astro-ph.CO].
- [5] P. Agrawal, B. Batell, P. J. Fox, and R. Harnik, “WIMPs at the Galactic Center,” *JCAP* **05** (2015) 011, [arXiv:1411.2592](https://arxiv.org/abs/1411.2592) [hep-ph].
- [6] F. Calore, I. Cholis, C. McCabe, and C. Weniger, “A Tale of Tails: Dark Matter Interpretations of the Fermi GeV Excess in Light of Background Model Systematics,” *Phys. Rev. D* **91** no. 6, (2015) 063003, [arXiv:1411.4647](https://arxiv.org/abs/1411.4647) [hep-ph].
- [7] A. Geringer-Sameth and S. M. Koushiappas, “Exclusion of canonical WIMPs by the joint analysis of Milky Way dwarfs with Fermi,” *Phys. Rev. Lett.* **107** (2011) 241303, [arXiv:1108.2914](https://arxiv.org/abs/1108.2914) [astro-ph.CO].
- [8] **Fermi-LAT** Collaboration, M. Ackermann *et al.*, “Constraining Dark Matter Models from a Combined Analysis of Milky Way Satellites with the Fermi Large Area Telescope,” *Phys. Rev. Lett.* **107** (2011) 241302, [arXiv:1108.3546](https://arxiv.org/abs/1108.3546) [astro-ph.HE].
- [9] **Fermi-LAT** Collaboration, M. Ackermann *et al.*, “Dark Matter Constraints from Observations of 25 Milky Way Satellite Galaxies with the Fermi Large Area Telescope,” *Phys. Rev. D* **89** (2014) 042001, [arXiv:1310.0828](https://arxiv.org/abs/1310.0828) [astro-ph.HE].
- [10] A. Geringer-Sameth, S. M. Koushiappas, and M. G. Walker, “Comprehensive search for dark matter annihilation in dwarf galaxies,” *Phys. Rev. D* **91** no. 8, (2015) 083535, [arXiv:1410.2242](https://arxiv.org/abs/1410.2242) [astro-ph.CO].
- [11] **Fermi-LAT** Collaboration, M. Ackermann *et al.*, “Searching for Dark Matter Annihilation from Milky Way Dwarf Spheroidal Galaxies with Six Years of Fermi Large Area Telescope Data,” *Phys. Rev. Lett.* **115** no. 23, (2015) 231301, [arXiv:1503.02641](https://arxiv.org/abs/1503.02641) [astro-ph.HE].
- [12] M. Di Mauro and M. W. Winkler, “Multimessenger constraints on the dark matter interpretation of the Fermi-LAT Galactic center excess,” *Phys. Rev. D* **103** no. 12, (2021) 123005, [arXiv:2101.11027](https://arxiv.org/abs/2101.11027) [astro-ph.HE].
- [13] B. Dutta, Y. Gao, T. Ghosh, and L. E. Strigari, “Confronting Galactic center and dwarf spheroidal gamma-ray observations with cascade annihilation models,” *Phys. Rev. D* **92** no. 7, (2015) 075019, [arXiv:1508.05989](https://arxiv.org/abs/1508.05989) [hep-ph].
- [14] A. Cuoco, J. Heisig, M. Korsmeier, and M. Krämer, “Probing dark matter annihilation in the Galaxy with antiprotons and gamma rays,” *JCAP* **10** (2017) 053, [arXiv:1704.08258](https://arxiv.org/abs/1704.08258) [astro-ph.HE].
- [15] K. K. Boddy, J. Kumar, L. E. Strigari, and M.-Y. Wang, “Sommerfeld-Enhanced J -Factors For Dwarf Spheroidal Galaxies,” *Phys. Rev. D* **95** no. 12, (2017) 123008, [arXiv:1702.00408](https://arxiv.org/abs/1702.00408) [astro-ph.CO].
- [16] M. Petac, P. Ullio, and M. Valli, “On velocity-dependent dark matter annihilations in dwarf satellites,” *JCAP* **12** (2018) 039, [arXiv:1804.05052](https://arxiv.org/abs/1804.05052) [astro-ph.GA].
- [17] K. K. Boddy, J. Kumar, and L. E. Strigari, “Effective J -factor of the Galactic Center for velocity-dependent dark matter annihilation,” *Phys. Rev. D* **98** no. 6, (2018) 063012, [arXiv:1805.08379](https://arxiv.org/abs/1805.08379) [astro-ph.HE].
- [18] K. K. Boddy, J. Kumar, J. Runburg, and L. E. Strigari, “Angular distribution of gamma-ray emission from velocity-dependent dark matter annihilation in subhalos,” *Phys. Rev. D* **100** no. 6, (2019) 063019, [arXiv:1905.03431](https://arxiv.org/abs/1905.03431) [astro-ph.CO].
- [19] K. K. Boddy, J. Kumar, A. B. Pace, J. Runburg, and L. E. Strigari, “Effective J -factors for Milky Way dwarf

- spheroidal galaxies with velocity-dependent annihilation,” *Phys. Rev. D* **102** no. 2, (2020) 023029, [arXiv:1909.13197 \[astro-ph.CO\]](#).
- [20] B. Boucher, J. Kumar, V. B. Le, and J. Runburg, “J-factors for velocity-dependent dark matter annihilation,” *Phys. Rev. D* **106** no. 2, (2022) 023025, [arXiv:2110.09653 \[hep-ph\]](#).
- [21] I. Z. Rothstein, T. Schwetz, and J. Zupan, “Phenomenology of Dark Matter annihilation into a long-lived intermediate state,” *JCAP* **07** (2009) 018, [arXiv:0903.3116 \[astro-ph.HE\]](#).
- [22] D. P. Finkbeiner and N. Weiner, “X-ray line from exciting dark matter,” *Phys. Rev. D* **94** no. 8, (2016) 083002, [arXiv:1402.6671 \[hep-ph\]](#).
- [23] S. Gori, S. Profumo, and B. Shakya, “Wobbly Dark Matter Signals at Cherenkov Telescopes from Long Lived Mediator Decays,” *Phys. Rev. Lett.* **122** no. 19, (2019) 191103, [arXiv:1812.08694 \[astro-ph.HE\]](#).
- [24] K. Agashe, S. J. Clark, B. Dutta, and Y. Tsai, “Nonlocal effects from boosted dark matter in indirect detection,” *Phys. Rev. D* **103** no. 8, (2021) 083006, [arXiv:2007.04971 \[astro-ph.CO\]](#).
- [25] L. M. Widrow, “Semi-analytic models for dark matter halos,” [arXiv:astro-ph/0003302](#).
- [26] L. E. Strigari, C. S. Frenk, and S. D. M. White, “Kinematics of Milky Way Satellites in a Lambda Cold Dark Matter Universe,” *Mon. Not. Roy. Astron. Soc.* **408** (2010) 2364–2372, [arXiv:1003.4268 \[astro-ph.CO\]](#).
- [27] J. F. Navarro, C. S. Frenk, and S. D. M. White, “The Structure of cold dark matter halos,” *Astrophys. J.* **462** (1996) 563–575, [arXiv:astro-ph/9508025](#).
- [28] A. B. Pace and L. E. Strigari, “Scaling Relations for Dark Matter Annihilation and Decay Profiles in Dwarf Spheroidal Galaxies,” *Mon. Not. Roy. Astron. Soc.* **482** no. 3, (2019) 3480–3496, [arXiv:1802.06811 \[astro-ph.GA\]](#).
- [29] K. Todoroki and M. V. Medvedev, “Dark matter haloes in the multicomponent model – I. Substructure,” *Mon. Not. Roy. Astron. Soc.* **483** no. 3, (2019) 3983–4003, [arXiv:1711.11078 \[astro-ph.CO\]](#).
- [30] K. Todoroki and M. V. Medvedev, “Dark matter haloes in the multicomponent model. III. From dwarfs to galaxy clusters,” *Mon. Not. Roy. Astron. Soc.* **510** no. 3, (2022) 4249–4264, [arXiv:2003.11096 \[astro-ph.CO\]](#).
- [31] K. T. E. Chua, K. Dibert, M. Vogelsberger, and J. Zavala, “The impact of inelastic self-interacting dark matter on the dark matter structure of a Milky Way halo,” *Mon. Not. Roy. Astron. Soc.* **500** no. 1, (2020) 1531–1546, [arXiv:2010.08562 \[astro-ph.GA\]](#).